



# Low Noise CMOS Amplifier for a Piezoresistive Magnetic Field Sensor

Norbert Dumas, Laurent Latorre, Pascal Nouet

## ► To cite this version:

Norbert Dumas, Laurent Latorre, Pascal Nouet. Low Noise CMOS Amplifier for a Piezoresistive Magnetic Field Sensor. DCIS: Design of Circuits and Integrated Systems, Nov 2003, Ciudad Real, Spain. pp.639-644. lirmm-00269472

**HAL Id: lirmm-00269472**

**<https://hal-lirmm.ccsd.cnrs.fr/lirmm-00269472>**

Submitted on 3 Apr 2008

**HAL** is a multi-disciplinary open access archive for the deposit and dissemination of scientific research documents, whether they are published or not. The documents may come from teaching and research institutions in France or abroad, or from public or private research centers.

L'archive ouverte pluridisciplinaire **HAL**, est destinée au dépôt et à la diffusion de documents scientifiques de niveau recherche, publiés ou non, émanant des établissements d'enseignement et de recherche français ou étrangers, des laboratoires publics ou privés.

# Low noise CMOS amplifier for a piezoresistive magnetic field sensor

Norbert DUMAS, Laurent LATORRE, Pascal NOUET

LIRMM / CNRS, University of Montpellier

**Abstract**— A two-axis MEMS magnetometer with integrated signal processing has been developed for a micro-compass application. The fabrication process is fully industrial and relies on bulk wet etching of CMOS dies. This technology offers cost-effective batch fabrication. Earth magnetic field measurement is achieved using piezoresistive gauges on a cantilever beam actuated by means of the Lorentz force. Due to low signal level available across the gauges, on-chip amplification with very high gain and low noise is then required. A fully differential amplifier based on a differential pair is suitable for this application. Circuit design approach is discussed in this paper. The obtained performances in terms of noise are compared to an instrumentation amplifier. Finally, a sensing resolution of  $0.9 \mu\text{T}$  is demonstrated with such a differential amplifier instead of  $2.1 \mu\text{T}$  resulting from standard-cell based instrumentation amplifier.

**Index Terms**— MEMS, CMOS AMPLIFIER, LOW NOISE, MONOLITHIC

## I. INTRODUCTION

### A. Magnetic field sensors for microcompass overview

An electronic compass requires the earth magnetic field measurement along at least two directions. Many magnetic field sensors have been developed in the last years. Hall sensors dominates the market and are usually only suitable for switching applications. This success is explained by low cost batch fabrication and integration with electronic. For example Hall sensors can be integrated with electronic in a CMOS process [1]. However low magnetic field measurement is a limitation. The lower magnetic field detectable with Hall device is about  $5 \mu\text{T}$  which is not enough for measuring earth magnetic field (about  $20 \mu\text{T}$  typically) with a sufficient resolution.

For measuring earth magnetic field Magneto Resistive (AMR) sensors are well represented on the market of electronic compass. Angle resolution lower than  $1^\circ$  are achieved with these sensors [2]. Manufacturers proposed application notes with external analog signal conditioning and angle computation using a micro-controller. Process fabrication of AMR sensor is non-standard and constitutes a limit for monolithic integration with electronic.

Flux gate and Giant Magneto Resistive (GMR) sensors are suitable to make very precise compass. However low cost

high-volume production is not possible with such specific technologies.

A single axis earth magnetic field measurement system has already been implemented with MEMS technology [3]. Using FSBM etching technique, an original monolithic compass with electronic for signal conditioning and computation is expected.

### B. MEMS technology

Front side bulk micromachining MEMS technology can be easily addressed in Europe through multi-project wafer services of CMP [4]. A  $0.8 \mu\text{m}$  standard CMOS process with two metal layers from Austria Mikro Systems [5] can be used. Sensor design and manufacturing is performed in two independent steps. First, a standard IC issued from a CMOS foundry is manufactured and second, wet etching of the obtained dies releases mechanical structures. Fig. 1 represents a cross-sectional schematic view of a CMOS process where polysilicon, metal and oxide layers are deposited over a substrate. According to designer requirements several dielectric-etching masks can be superimposed to leave the silicon bulk uncovered at the end of the standard CMOS process. Then, post-process operates as an anisotropic silicon etching that uses the various oxide layers as natural mask. Suspended structures such as cantilever beams, bridges or membranes are finally obtained.

According to our experience, this process is the cheapest way to release mechanical structures from CMOS dies. Also, reliability of suspended beams has been measured and found excellent.

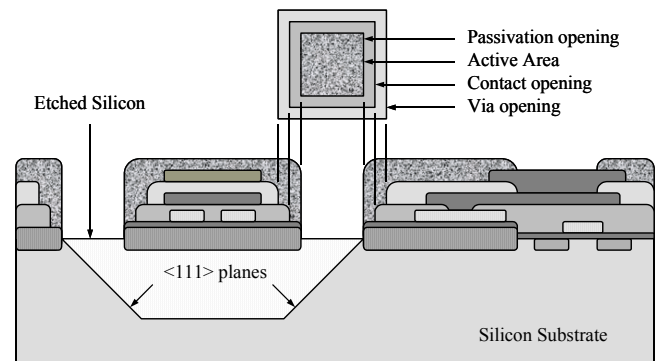


Fig. 1 Cross sectional view of a CMOS process

### C. Sensing principle

The proposed mechanical structure [6], schematically represented in Fig. 2, is a U-shaped cantilever beam. An electrical current ( $I$ ) pass through the beam by means of aluminum planar coils. Lorentz force ( $F$ ) results from the interaction between a magnetic field ( $B$ ) and  $I$ . This force depends on the width ( $W_c$ ) of the cantilever :  $F = I \times W_c \times B$

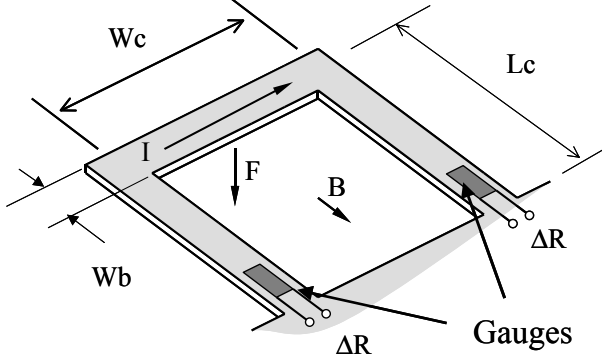


Fig. 2 Schematic of the U-shaped cantilever

This electromagnetic force is used to deform the mechanical structure. Relation between the position ( $z$ ) of the bent extremity of the cantilever and the Lorentz force is described by the equation :

$$M \frac{d^2 z}{dt^2} = -K \cdot z - D \frac{dz}{dt} + F$$

Where  $M$  is the mass of the mechanical structure,  $K$  the stiffness and  $D$  the damping factor. It is a second order spring-mass-damper system. The deformation is then translated into a resistance variation ( $\Delta R$ ) by means of embedded polysilicon strain gauges with a nominal resistance value  $R$ . The entire system, with a calibrated current  $I$ , can be represented as a transfer function between the magnetic induction and the resistance variation. The frequency response, shown on Fig. 3, has a resonance frequency peak ( $f_0$ ).

The gauges are placed in a Wheatstone bridge with two others resistors in order to translate the resistance variation into a voltage variation.

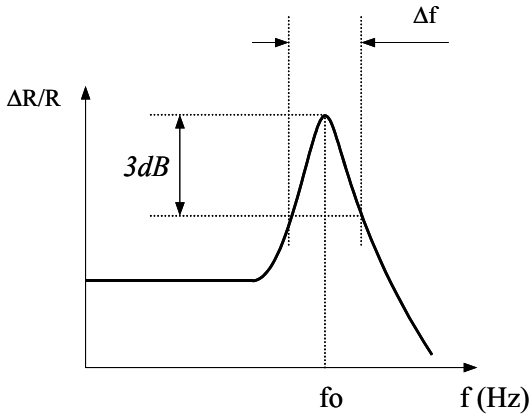


Fig. 3 Frequency response of the U-shaped cantilever

Two modes of actuation can be used for measuring magnetic field. The first one is a static mode and uses a calibrated dc current ( $I$ ). The voltage level at the output of the Wheatstone bridge is directly proportional to the magnetic induction. The ratio between the voltage level and the magnetic induction is the static sensitivity ( $S_{stat}$ ). The working frequency is null and then,  $1/f$  noise coming from MOS transistor devices used to amplified the output signal strongly limits the resolution of the sensor.

The other actuation mode make use of an alternative current for  $I$ . The amplitude of the output signal is then modulated by the value of the static (or low frequency) magnetic induction. The ratio between the output amplitude and the magnetic induction then represents the sensitivity. The best sensitivity is obtained with an actuation current frequency equal to the resonance frequency ( $f_0$ ) of the mechanical structure. The relation between the resonant sensitivity ( $S_{res}$ ) and  $S_{stat}$  depends on the quality factor ( $Q$ ) :

$$\frac{S_{res}}{S_{stat}} = \frac{f_0}{\Delta f} = Q$$

Resonant actuation mode takes benefit from the high- $Q$  factor of the structure. In addition to that the working frequency is preferable for  $1/f$  noise consideration. The actuation mode used for the presented microcompass is then resonant.

Design parameters, such as cantilever dimension and number of turns in the coil, have been optimized to have the better relative sensitivity (sensitivity/consumption ratio) possible. These are presented in Table 1 with the resulting sensor parameters.

TABLE 1  
DESIGN PARAMETER SET

Design parameter	Designation	Value
$W_c$	Cantilever width	320 $\mu\text{m}$
$L_c$	Cantilever length	320 $\mu\text{m}$
$W_b$	Single Beam width	120 $\mu\text{m}$
$N$	Number of turns in the coil	59
$I$	Peak to peak total current through the beam	118 mApp
$I_f$	Peak to peak supply current for actuation ( $I = N \times I_f$ )	2 mApp
SENSOR PARAMETERS		
Sensor parameter	Designation	Value
$K$	Stiffness	12.6 $\text{N m}^{-1}$
$M$	Mass	$6.3 \times 10^{-10}$ kg
$D$	Damping factor	$7.83 \times 10^{-7}$ N s $\text{m}^{-1}$
$f_0$	Resonant frequency	22.5 kHz
$Q$	Quality factor	114
$S_{res}$	Resonant sensitivity	0.85 $\text{Vrms/T}$
$S_{res(rel)}$	Relative resonant sensitivity	425 $\text{Vrms/(T A)}$
$Tr$	Response time	10 ms

### D. System overview :

Fig.4 presents the complete system for measuring the azimuth ( $\theta$ ) that is the angle between the direction of the North and the reference axis of the sensor. Two cantilevers are in orthogonal configuration in order to measure

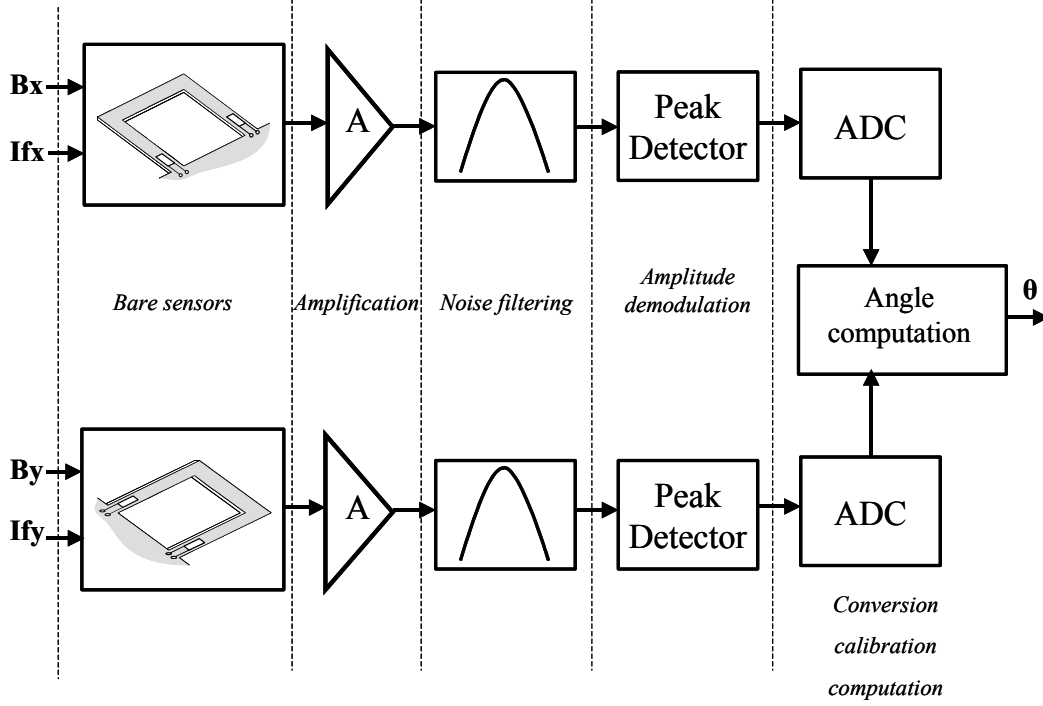


Fig. 4 Block diagram of the compass system

earth magnetic field along two directions (Bx and By) in the horizontal plane. The bare sensor part includes the cantilever with gauges in a Wheatstone bridge configuration. Analog signal treatments for each axis are separated. Band-pass filters are centered on the working resonance frequency 22.5 kHz. Its function is to attenuate noise spectral density outside the bandwidth. Angle computation and calibration is achieved with digital electronic.

We consider that angle calculation need to be refreshed at least each 1s. The response time of the cantilever (about 10ms) is good enough for this specification. A narrow bandwidth is then required for the filter for good noise filtering performance. However the filter bandwidth has to be large enough to be sure it will match mechanical resonance, taking into account scattering on the mechanical resonance frequency and scattering on the specification of the filter itself. We consider here that the filter is not adjustable. Standard deviation of the resonance frequency found by characterization is around 6%. It leads to a maximum filter bandwidth of 2.7 kHz if only mechanical scattering are taken into consideration. To take into account filter scattering the specified bandwidth of the filter is 6kHz.

We will see that the resolution limit due to the bare sensor part is 0.6  $\mu\text{T}$ . It leads to an angle resolution of about  $3^\circ$ . In order to preserve this resolution the small-signal level available across the gauges (17  $\mu\text{V}_{\text{rms}}$  for  $B = 20\mu\text{T}$ ) has to be strongly amplified before treatment. First stage of the amplification circuitry has to be carefully designed. It is achieved by a fully differential amplifier with size of transistors optimized for noise reduction.

## II. DESIGN APPROACH AND NOISE CONSIDERATION

The following section introduces the noise models that has been used in the noise analysis [7]. Using a differential structure for amplification we consider that power supply noise and other common mode noises are rejected. This assumption will be verified with PSRR and CMMR evaluation in the last section of this paper.

### A. Thermal-mechanical noise

It usually limits the resolution of very small cantilevers [8]. It is due to molecular agitation of air surrounding the cantilever. It is a physical equivalent to Johnson noise in resistors and can be modeled by adding a random force across the damper. The spectral density of mechanical noise is given by :

$$\overline{F_n^2}(f) = 4 \times k \times T \times D \text{ (N}^2/\text{Hz)}$$

Where  $k = 1.38 \times 10^{-23} \text{ JK}^{-1}$  is the Boltzman's constant,  $T$  the temperature and  $D$  the damping factor.

The shape of the noise spectrum at the system output depends on the cantilever transfer function which is equivalent to a band pass filter of 200 Hz bandwidth. With the characterized value  $D = 7.8 \times 10^{-7} \text{ kg/s}$  it leads to a RMS fluctuation force  $F_n$ , at room temperature of :

$$F_n = \sqrt{4 \times 1.38 \times 10^{-23} \times 300 \times 7.8 \times 10^{-7} \times 200} = 1.61 \text{ pN}$$

This noise is equivalent to a magnetic induction noise usually called NEMI (Noise Equivalent Magnetic Induction). It is defined by ratio between the output noise and the absolute sensitivity :

$$NEMI = \frac{F_n}{I \times W_c} = 43 \text{ nT}$$

This value is an evaluation of the resolution considering only mechanical noise. We will see that, compared to the various sources of electrical noise, thermal-mechanical noise is not a limiting factor of the resolution.

### B. Thermal noise from Wheatstone bridge

Thermal noise that comes from the gauges limits the resolution of the sensor. It is due to thermal agitation of charge carriers in the resistors. The noise spectral density generated by each resistor is :

$$\bar{V}_n^2(f) = 4kTR \text{ (V}^2/\text{Hz)}$$

Where R the resistance value.

The spectral noise density due to the four resistors in a Wheatstone bridge configuration is equivalent to only one resistor. The value of R is chosen considering the power consumption that is  $V_{dd}^2/R$ . A resistance of 2 kOhms has been calculated to equalize the power consumption of the cantilever actuation. The total output noise is given by integrating the output noise on a bandwidth (BW) of 6kHz, considering that the signal is observed through a filter. The resulting NEMI gives the resolution :

$$NEMI = \frac{\sqrt{4 \times k \times T \times R \times BW}}{S_{res}} = 0.6 \mu T$$

Thermal noise is much higher than thermal-mechanical noise. Power supply and substrate noises are rejected by the differential configuration of the Wheatstone bridge. The resolution inherent to the bare sensor is then  $0.6 \mu T$  and comes mainly from the gauges.

### C. MOS transistor noise

It is the main source of noise found in amplifiers. Two sources of noise dominates in a MOS transistors operating in active region : thermal and flicker noise. Thermal noise is due to the resistive channel. This noise could be modeled as a white noise voltage source in series with the gate of a noiseless transistor. The noise spectral density of this source is given by :

$$\bar{V}_{tn}^2(f) = 4 \times k \times T \times \left(\frac{2}{3}\right) \times \frac{1}{g_m} \text{ (V}^2/\text{Hz)}$$

Where  $g_m$  the small-signal transconductance. We see that if the gate is considered to be the input of an amplifier the thermal noise can be reduced by choosing a high transconductance value. This implies large W/L ratio.

Flicker noise is found in any active device. It is caused by traps for carriers that are located at the boundary between the Si and SiO<sub>2</sub>. It is modeled as a voltage source in series with the gate. The noise spectral density decreases with the frequency value :

$$\bar{V}_{fn}^2(f) = \frac{K}{W \times L \times Cox \times f} \text{ (V}^2/\text{Hz)}$$

Where  $W$  is the width of the channel and  $L$  the length.  $K$  is a factor that depends of the technology. It is lower for PMOS transistor in comparison with NMOS transistor. This noise is reduced using large surface  $W \times L$ .

### D. Noise analysis of a CMOS differential pair :

The proposed amplifier is based on a CMOS differential pair with active loads. Fig. 5 is an equivalent schematic of this amplifier with transistors and their equivalent input sources of noise.

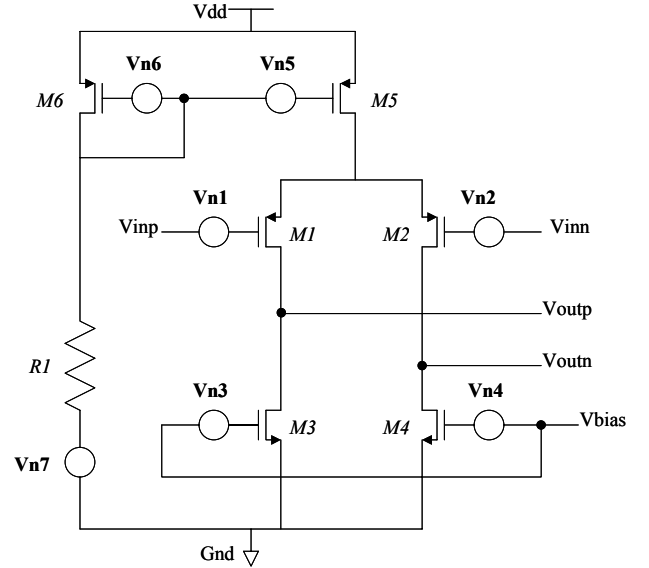


Fig. 5 Equivalent schematic of the differential pair amplifier

Vinn and Vinp are the differential inputs whereas Voutp and Voutn the differential outputs. Vbias is the biasing voltage for the active loads. Fully differential configuration helps rejecting the common mode sources of noise such as power supply, biasing voltage and substrate noises. Ideally, common mode noise rejection is infinite. In fact it is limited by unmatched input transistors ( $M1$  and  $M2$ ) and between active loads ( $M3$  and  $M4$ ). Transistors sizes are designed to have a NEMI equal to the resolution of the bare sensor considering a noise bandwidth of 6 kHz. The equivalent circuit using noise equivalent model for transistors and resistors is given on Fig. 3. PMOS has been chosen for the input transistors because of their low flicker noise.  $M5$ ,  $M6$  and  $M7$  generates common mode noise inputs regarding the output signal so noise will be rejected. Total equivalent input noise is given by :

$$\bar{V}_{n^2}(f) = \bar{V}_{n1}^2(f) + \bar{V}_{n2}^2(f) + \left(\frac{g_{m1}}{g_{m4}}\right)^2 \times (\bar{V}_{n3}^2(f) + \bar{V}_{n4}^2(f))$$

TABLE 2

NOISE FROM INPUT TRANSISTORS IN FUNCTION OF CHANNEL WIDTH				
Channel width $W$ ( $\mu\text{m}$ )	100	200	400	800
Spectral noise density due to thermal agitation in M1 and M2 : $\bar{V}_{t_{n1}}^2(f) + \bar{V}_{t_{n2}}^2(f)$ (aV/Hz)	212	106	52	26
NEMI ( $\mu\text{T}$ )	1.3	0.95	0.65	0.46

• The two sources of noise  $V_{n1}$  and  $V_{n2}$  are inherent to the input transistors. The noise generated by these two sources can be reduced by sizing these transistors. Table 2 gives the thermal noise density, due to both input transistors, and the corresponding NEMI at different widths ( $W$ ). Length of the transistors is settled to  $8\mu\text{m}$ . NEMI is calculated by integrating the white noise spectral density on a bandwidth of 6kHz and dividing this value by the sensitivity of the bare sensor.

$W = 400\mu\text{m}$  is finally chosen to have a NEMI due to thermal noise smaller than  $1\mu\text{T}$ .

For this size of input transistors, the corresponding flicker noise contribution is negligible (2%). Noise contribution is defined as the ratio between the noise spectral density due the contributor and the total noise spectral density. It is evaluated with simulation tools.

• Flicker noise inherent to  $M3$  and  $M4$  is reduced by choosing  $W*L$  big enough. In addition noise contribution from these two transistors is minimized by choosing  $W/L$  small enough. With  $W = 42\mu\text{m}$  and  $L = 32\mu\text{m}$  noise contribution of active load is 30%. This noise comes from thermal noise for about 50% and from flicker noise for about 50%.

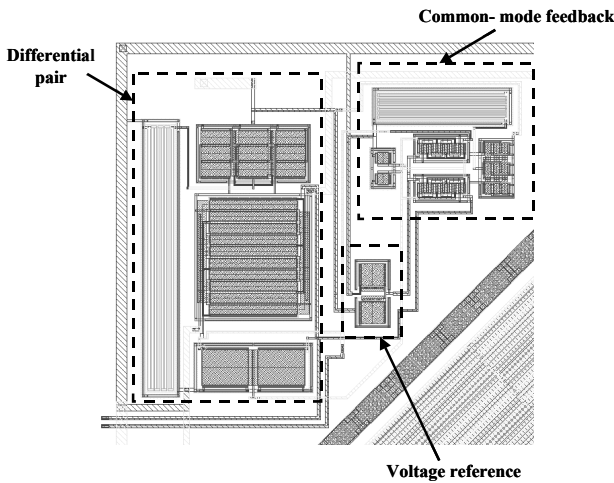


Fig. 6 Fully differential amplifier layout

### III. PERFORMANCE OF THE PROPOSED AMPLIFIER

The amplifier needs a  $V_{\text{bias}}$  reference voltage for the active load. As the output voltage is very sensitive to  $V_{\text{bias}}$ , it can't be generated independently from the output. That is the reason for a Common Mode Feed Back circuit (CMFB) to be added. The reference voltage needed for this circuit is generated using two diode-connected PMOS transistor. The total surface required is  $0,07\text{ mm}^2$  for the amplifier alone (Fig. 6) and  $2\text{ mm}^2$  for the two axis sensor with integrated amplification (Fig. 7).

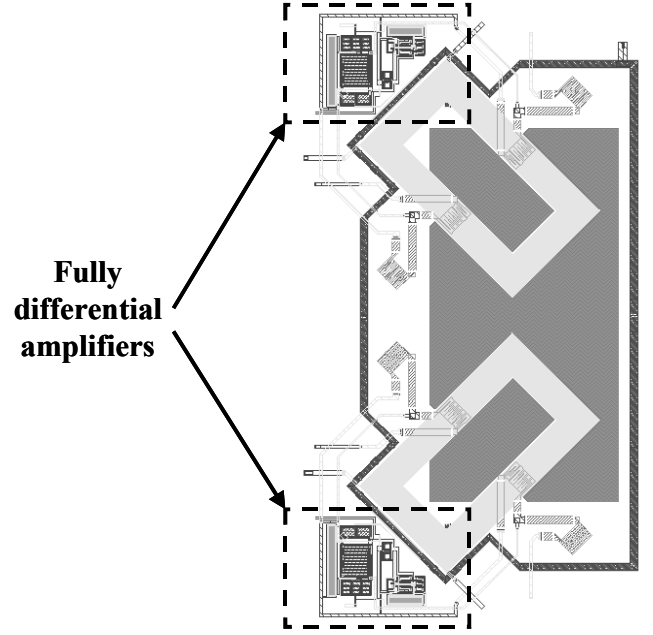


Fig. 7 Layout of the 2-axis sensor with amplifiers

The proposed amplifier has been compared to an instrumentation amplifier commonly used for signal treatment amplification (Table 3). The operational amplifier is chosen among available standard cells in the foundry design kit. It is given with low noise and low offset characteristics. Schematic of the instrumentation amplifier structure is given on Fig. 8.

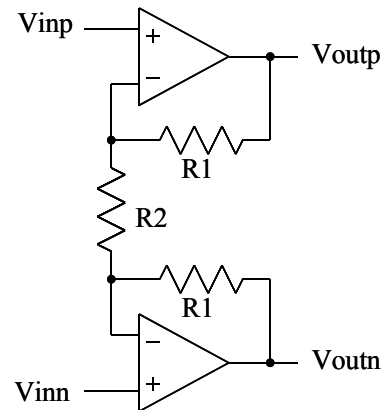


Fig. 8 Schematic of the instrumentation amplifier

TABLE 3  
COMPARISON OF THE PROPOSED AMPLIFIER WITH AN  
INSTRUMENTATION AMPLIFIER

	Instrumentation amplifier	Fully Differential Amplifier
Gain	102	357
Equivalent noise input density at 22,5 kHz	570 aV <sup>2</sup> /Hz	63 aV <sup>2</sup> /Hz
NEMI with a 6kHz noise Bandwidth	2 $\mu$ T	0,7 $\mu$ T
Surface	0,3 mm <sup>2</sup>	0,07 mm <sup>2</sup>
CMRR	84 dB	76 dB
PSRR	83 dB	81 dB

- Noise of instrumentation amplifier comes mainly from the four input transistors pair of the first stage of the operational amplifiers (48%) and from the four active loads of this first stage (40%). Differences in terms of noise come from the number of transistors required at the input and their intrinsic noise. Each AOP input transistors generate 68 aV<sup>2</sup>/Hz because of their size  $W = 600 \mu\text{m}$  and  $L = 24 \mu\text{m}$ .

- We see that performances in terms of surface and gain are better for the amplifier pair. Instrumentation amplifier gain is limited by unity gain bandwidth of the operational amplifiers ( $BW_{op}$ ). As the working frequency is 22.5 kHz the cut-off frequency ( $F_c$ ) of the amplifier must be higher. The maximum gain value ( $G_{max}$ ) is given by :

$$G_{max} = \frac{BW_{op}}{F_c}$$

With  $F_c = 32.5 \text{ kHz}$  and  $BW_{op} = 3.4 \text{ MHz}$  the maximum gain is about 100. High gain with instrumentation amplifier requires several stages.

- In terms of Common Mode Rejection Ratio and Power Supply Rejection Ratio both circuits are equivalent. These two parameters depends of device matching. They have been evaluated using a Monte Carlo statistical analysis taking into account mismatch. These values are good enough to consider that power supply noise and others common-mode noises are rejected. The limiting factor for resolution is then the noise inherent to devices, as it has been previously supposed.

- The main drawback of the amplifier pair is temperature dependence of gain. The gain ( $G$ ) depends of small signal parameters that are sensitive to temperature. It is given by :

$$G = g_{m1} \times (rds_1 // rds_3)$$

Where  $rds_1$  and  $rds_3$  are the dynamical resistances seen between the drain and the source of transistors  $M1$  and  $M3$ .  $g_{m1}$  is the transconductance value of transistor  $M1$ . For a compass application, gain fluctuation is eliminated with angle

calculation. Azimuth is not dependent of the amplification factor if fluctuations are equal on both axis. Due to symmetrical layout and small dimension one can consider that this condition is verified.

#### IV. CONCLUSION

Noise analysis on a sensor including electronic has been presented. An amplifier based on a CMOS differential pair is found to be have better performance than a conventional instrumentation amplifier. Resolution of  $1 \mu\text{T}$  has been calculated using this proposed amplifier. Using this amplification structure , an original, fully monolithic, CMOS micro-compass will be fabricated.

#### REFERENCES

- [1] Vincent Frick, Luc Hebrard, Philippe Poure, Fancis Braun "Design, Characterisation, Modeling and Performances of Magnetic Sensors in Standard CMOS Technology", Proc. Of DCIS 2000, pp. 700-704, Nov. 2000.
- [2] Micheal J. Caruso, M. Missous, "Applications of Magnetoresistive Sensors in Navigation Systems", Technical articles, Honeywell Inc. <http://www.magneticsensors.com/>
- [3] Vincent Berouille, Yves Bertrand, Laurent Latorre, Pascal Nouet, "Monolithic piezoresistive CMOS magnetic field sensors", Sensors and actuators A 103 (2003) 23-32.
- [4] Ciciuits Multi-Projets (CMP) is a broker in Ics, MCMs and MEMS. <http://cmp.imag.fr/>
- [5] <http://www.austriamicrosystems.com/>
- [6] L. Latorre, V. Berouille Y. Bertrand, I. Salesse and P. Nouet. "Electro Mechanical Magnetic Field sensors" Proc. Of DCIS 2000, p. 694-699, 2000.
- [7] David A. Johns, Ken Martin, "Analog integrated circuit design", John Wiley & Sons, Inc., 1997, pp. 199.
- [8] Thomas B. Gabrielson, "Mechanical, thermal noise in micromachined acoustic and vibration sensors", IEEE Trans. Electron Devices, VOL. 40, NO. 5, May 1993.